EVA: GPS-based extended velocity and acceleration determination

**Dagoberto Salazar · Manuel Hernandez-Pajares ·
Jose Miguel Juan-Zornoza · Jaume Sanz-Subirana ·
Angela Aragon-Angel**

Abstract In this work, a new GPS carrier phase-based
velocity and acceleration determination method is presented
that extends the effective range of previous techniques. The
method is named 'EVA', and may find applications in fields
such as airborne gravimetry when rough terrain or water bod-
ies make difficult or impractical to set up nearby GPS refer-
ence receivers. The EVA method is similar to methods such
as Kennedy (Precise acceleration determination from carrier
phase measurements. In: Proceedings of the 15th interna-
tional technical meeting of the satellite division of the Insti-
tute of Navigation. ION GPS 2002, Portland pp 962–972,
2002b) since it uses L1 carrier phase observables for veloc-
ity and acceleration determination. However, it introduces
a wide network of stations and it is independent of pre-
cise clock information because it estimates satellite clock
drifts and drift rates 'on-the-fly', requiring only orbit data
of sufficient quality. Moreover, with EVA the solution rate
is only limited by data rate, and not by the available pre-
cise satellite clocks data rate. The results obtained are more
robust for long baselines than the results obtained with the
reference Kennedy method. An advantage of being indepen-
dent of precise clock information is that, beside IGS Final
products, also the Rapid, Ultra-Rapid (observed) and Ultra-
Rapid (predicted) products may be used. Moreover, the EVA
technique may also use the undifferenced ionosphere-free
carrier phase combination (LC), overcoming baseline limi-
tations in cases where ionosphere gradients may be an issue
and very low biases are required. During the development of
this work, some problems were found in the velocity esti-
mation process of the Kennedy method. The sources of the

problems were identified, and an improved version of the
Kennedy method was used for this research work. An exper-
iment was performed using a light aircraft flying over the Py-
renees, showing that both EVA and the improved Kennedy
methods are able to cope with the dynamics of mountain-
ous flight. A RTK-derived solution was also generated, and
when comparing the three methods to a known zero-velocity
reference the results yielded similar performance. The EVA
and the improved-Kennedy methods outperformed the RTK
solutions, and the EVA method provided the best results in
this experiment. Finally, both the improved version of the
Kennedy method and the EVA method were applied to a net-
work in equatorial South America with baselines of more
than 1,770 km, and during local noon. Under this tough sce-
nario, the EVA method showed a clear advantage for all com-
ponents of velocity and acceleration, yielding better and more
robust results.

1 Introduction

Several methods may be used to obtain GNSS-based velocity
and acceleration. A common method is by time-differenti-
ating successive position solutions of the moving vehicle.
However, this approach has several disadvantages, such as:
the velocity and acceleration precision are strongly depen-
dent on position accuracy and the gain or loss of a satellite
can introduce discontinuities (Bruton 2000).

Another common approach is to use the Doppler observ-
able, when available (see, for instance, the work by Parkinson
and Spilker Jr. 1996). The problem in this method is that
the raw Doppler observable can be much noisier than the

D. Salazar (✉) · M. Hernandez-Pajares · J. M. Juan-Zornoza ·
J. Sanz-Subirana · A. Aragon-Angel
gAGE/UPC Research group of Astronomy and Geomatics,
Barcelona, Spain
e-mail: Dagoberto.Jose.Salazar@upc.edu

Table 1 Velocity sigmas for static and flight tests according to van Graas and Soloviev (2004)

	Static mode (mm/s)	Low dynamics test flight (mm/s)
U	7.9	9.7
E	2.2	2.6
N	3.1	3.7

Doppler value obtained by differentiating the carrier phase observable (see Cannon et al. 1997; Szarmes et al. 1997; Hofmann-Wellenhof et al. 2008).

A different method was proposed by van Graas and Soloviev (2004), where differences between consecutive *epochs* of carrier phase observables were used. This paper reported standard deviations of velocity noise for static mode and for a DC-3 aircraft test flight with low dynamics, using a position-based, DGPS-based solution as reference. Results are presented in Table 1.

A fourth approach, related to the former and the one to be examined in this work, is to use the carrier phase as an observable and to numerically differentiate it to get both range rate and range acceleration. This method is focused on acceleration estimation for airborne gravimetry purposes and was presented in Jekeli (1994) and Jekeli and Garcia (1997), and later expanded by Kennedy (2002b).

The main objective of this work is to extent the range of the Kennedy (2002b) technique using a network of reference stations with long baselines, and estimating the satellite clock drifts and drift rates 'on-the-fly'. This strategy allows the use of different IGS products, like the Ultra-Rapid (predicted) products. It should be noted, however, that the new technique has been tested only in post-process mode.

2 Carrier phase method fundamentals

The work of Jekeli and Garcia (1997) implemented the carrier phase method using the measurements from only four satellites. The former method was later expanded by Kennedy (2002a,b) to incorporate all available measurements, and to add a covariance model to weight them. The Kennedy (2002b) method explanation starts with the geometry set up in Fig. 1.

2.1 Velocity determination

From Fig. 1 it can be seen that:

$$\rho_m^p = \mathbf{e}_m^p \cdot \mathbf{x}_m^p, \tag{1}$$

where ρ_m^p is the geometric distance between SV^p and RX_m antenna phase centers, and $\mathbf{e}_m^p$ is the unit vector in the RX_m-SV^p direction. Satellite SV^p will be the *reference satellite*.
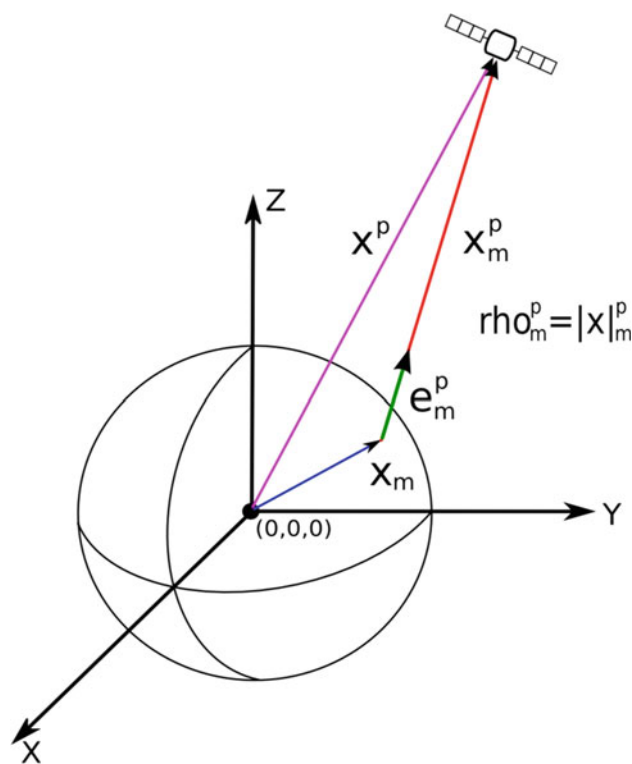
Fig. 1 RX-SV geometry for carrier phase method

Another equation closely related to Eq. 1 that can be deduced from Fig. 1 is:

$$\mathbf{x}_m^p = \rho_m^p \mathbf{e}_m^p. \tag{2}$$

Differentiating Eq. 1, it yields:

$$\dot{\rho}_m^p = \dot{\mathbf{e}}_m^p \cdot \mathbf{x}_m^p + \mathbf{e}_m^p \cdot \dot{\mathbf{x}}_m^p \tag{3}$$

If we substitute Eq. 2 into Eq. 3, the later becomes:

$$\dot{\rho}_m^p = \rho_m^p (\dot{\mathbf{e}}_m^p \cdot \mathbf{e}_m^p) + \mathbf{e}_m^p \cdot \dot{\mathbf{x}}_m^p. \tag{4}$$

However, $\dot{\mathbf{e}}_m^p$ and $\mathbf{e}_m^p$ are orthogonal, so Eq. 4 becomes:

$$\dot{\rho}_m^p = \mathbf{e}_m^p \cdot \dot{\mathbf{x}}_m^p. \tag{5}$$

Now, introducing an additional satellite SV^q:

$$\dot{\rho}_m^q = \mathbf{e}_m^q \cdot \dot{\mathbf{x}}_m^q. \tag{6}$$

Carrying out single differences between SV^q and SV^p satellites:

$$\nabla \dot{\rho}_m^{q,p} = \mathbf{e}_m^q \cdot \dot{\mathbf{x}}_m^q - \mathbf{e}_m^p \cdot \dot{\mathbf{x}}_m^p \implies$$
$$\nabla \dot{\rho}_m^{q,p} = \mathbf{e}_m^q \cdot \dot{\mathbf{x}}^q - \mathbf{e}_m^q \cdot \dot{\mathbf{x}}_m - (\mathbf{e}_m^p \cdot \dot{\mathbf{x}}^p - \mathbf{e}_m^p \cdot \dot{\mathbf{x}}_m) \implies$$
$$\nabla \dot{\rho}_m^{q,p} + \mathbf{e}_m^p \cdot \dot{\mathbf{x}}^p = \mathbf{e}_m^q \cdot \dot{\mathbf{x}}^q - \mathbf{e}_m^q \cdot \dot{\mathbf{x}}_m + \mathbf{e}_m^p \cdot \dot{\mathbf{x}}_m. \tag{7}$$

Subtracting $\mathbf{e}_m^p \cdot \dot{\mathbf{x}}^q$ from both sides of Eq. 7, it yields:

$$\nabla \dot{\rho}_m^{q,p} + \mathbf{e}_m^p \cdot (\dot{\mathbf{x}}^p - \dot{\mathbf{x}}^q) = (\mathbf{e}_m^q - \mathbf{e}_m^p) \cdot \dot{\mathbf{x}}_m^q \tag{8}$$

In Equation 8, if the position of the receiver is known with an accuracy better than a few meters, the direction vectors $\mathbf{e}_m^q$ and $\mathbf{e}_m^p$ could be computed without affecting the results (Jekeli 1994). The satellite velocities $\dot{\mathbf{x}}^p$ and $\dot{\mathbf{x}}^q$ are needed and may be computed by different methods (see Sect. 3), and the unknown is $\dot{\mathbf{x}}_m^q$. The formula requires the $\nabla \dot{\rho}_m^{q,p}$ term. In order to compute it, let's present the expression for carrier phase measurements ϕ_m^p between satellite p and receiver m):

$$\begin{aligned} \phi_m^p = {} & \rho_m^p + c(dt_m - dt^p) + rel_m^p + T_m^p - \alpha_f I_m^p \\ & + b_m^p + \omega_{\phi,m}^p + m_{\phi,m}^p + \varepsilon_{\phi,m}^p, \end{aligned} \quad (9)$$

where ρ_m^p is the geometric distance between SV^p and RX_m antenna phase centers, dt^p and dt_m are the offset of SV and RX clocks regarding to GPS Time, respectively, rel_m^p is the bias due to relativistic effects (linked to SV^p orbit eccentricity), T_m^p is the tropospheric delay, $\alpha_f I_m^p$ is the effect due to the ionospheric delay, b_m^p is the phase ambiguity term, including the carrier phase instrumental delays, $\omega_{\phi,m}^p$ is the *wind-up* effect, $m_{\phi,m}^p$ is the multipath effect, and $\varepsilon_{\phi,m}^p$ is the unmodeled noise for the phase measurement (in the millimeter range).

The method by Kennedy (2002b) uses the carrier phase measurements in L1 frequency due to wider availability and lower noise than L2 measurements and LC (ionosphere-free) combination.

Differentiating Eq. 9 regarding time, and assuming that *no cycle slip occurs* and receiver clock millisecond adjustments are properly being taken care of, the phase ambiguity term and most part of systematic errors and slow-varying terms are removed, resulting into:

$$\dot{\phi}_m^p = \dot{\rho}_m^p + c(\dot{d}t_m - \dot{d}t^p) + \dot{T}_m^p - \alpha_f \dot{I}_m^p + \dot{\varepsilon}_{\phi,m}^p, \quad (10)$$

where the $\dot{\varepsilon}_{\phi,m}^p$ noise term absorbs the higher order terms.

It must be noted that proper cycle slips detection algorithms must be in place. When a cycle slip is detected, the affected satellite is taken out of the equation system for as long as this condition remains.

In order to eliminate the clock drift and atmosphere-induced effects, a reference station k may be included, resorting to double differencing of Eq. 10 between *nearby* receivers. This yields the approximation stated in Eq. 11.

$$\Delta \nabla \dot{\phi}_{m,k}^{q,p} \simeq \Delta \nabla \dot{\rho}_{m,k}^{q,p}. \quad (11)$$

From Eq. 11 an approximation for term $\nabla \dot{\rho}_m^{q,p}$ is obtained:

$$\nabla \dot{\rho}_m^{q,p} \simeq \Delta \nabla \dot{\phi}_{m,k}^{q,p} + \nabla \dot{\rho}_k^{q,p}, \quad (12)$$

where the term $\nabla \dot{\rho}_k^{q,p}$ is accurately known because it belongs to reference station k. Substituting Eq. 12 into Eq. 8 and rearranging terms, it will yield Eq. 13, which is the expression used to compute the rover receiver velocity:

$$\Delta \nabla \dot{\phi}_{m,k}^{q,p} + \nabla \dot{\rho}_k^{q,p} + \mathbf{e}_m^p \dot{\mathbf{x}}^p - \mathbf{e}_m^q \dot{\mathbf{x}}^q = (\mathbf{e}_m^p - \mathbf{e}_m^q) \cdot \dot{\mathbf{x}}_m. \quad (13)$$

2.2 Acceleration determination

In order to obtain an expression for carrier phase-based acceleration, Eq. 5 is differentiated a second time:

$$\ddot{\rho}_m^p = \mathbf{e}_m^p \cdot \ddot{\mathbf{x}}_m^p + \dot{\mathbf{e}}_m^p \cdot \dot{\mathbf{x}}_m^p. \quad (14)$$

And differentiation of Eq. 2 yields:

$$\dot{\mathbf{x}}_m^p = \dot{\rho}_m^p \mathbf{e}_m^p + \rho_m^p \dot{\mathbf{e}}_m^p. \quad (15)$$

From Eq. 15, the term $\dot{\mathbf{e}}_m^p$ can be found:

$$\dot{\mathbf{e}}_m^p = \frac{1}{\rho_m^p} \left[\dot{\mathbf{x}}_m^p - \dot{\rho}_m^p \mathbf{e}_m^p \right]. \quad (16)$$

Substituting Eq. 16 into Eq. 14 yields:

$$\ddot{\rho}_m^p - \mathbf{e}_m^p \cdot \ddot{\mathbf{x}}^p - \frac{1}{\rho_m^p} \left[|\dot{\mathbf{x}}_m^p|^2 - (\dot{\rho}_m^p)^2 \right] = -\mathbf{e}_m^p \cdot \ddot{\mathbf{x}}_m. \quad (17)$$

Introducing an equation for an additional satellite SV^q, and carrying out single differences between satellites SV^q and SV^p:

$$\begin{aligned} & \nabla \ddot{\rho}_m^{q,p} - \mathbf{e}_m^q \cdot \ddot{\mathbf{x}}^q + \mathbf{e}_m^p \cdot \ddot{\mathbf{x}}^p - \frac{1}{\rho_m^q} \left[|\dot{\mathbf{x}}_m^q|^2 - (\dot{\rho}_m^q)^2 \right] \\ & + \frac{1}{\rho_m^p} \left[|\dot{\mathbf{x}}_m^p|^2 - (\dot{\rho}_m^p)^2 \right] = -(\mathbf{e}_m^q - \mathbf{e}_m^p) \cdot \ddot{\mathbf{x}}_m. \end{aligned} \quad (18)$$

Now, Equation 12 is differentiated again:

$$\nabla \ddot{\rho}_m^{q,p} \simeq \Delta \nabla \ddot{\phi}_{m,k}^{q,p} + \nabla \ddot{\rho}_k^{q,p}. \quad (19)$$

And substituting Eq. 19 into Eq. 18 and rearranging yields the expression for the carrier phase-based acceleration:

$$\begin{aligned} & \Delta \nabla \ddot{\phi}_{m,k}^{q,p} + \nabla \ddot{\rho}_k^{q,p} + \mathbf{e}_m^p \cdot \ddot{\mathbf{x}}^p - \mathbf{e}_m^q \cdot \ddot{\mathbf{x}}^q \\ & + \frac{1}{\rho_m^p} \left[|\dot{\mathbf{x}}_m^p|^2 - (\dot{\rho}_m^p)^2 \right] - \frac{1}{\rho_m^q} \left[|\dot{\mathbf{x}}_m^q|^2 - (\dot{\rho}_m^q)^2 \right] \\ & = (\mathbf{e}_m^p - \mathbf{e}_m^q) \cdot \ddot{\mathbf{x}}_m. \end{aligned} \quad (20)$$

Note that the rover velocity is a prerequisite to compute the acceleration. This is evident in terms like $\dot{\mathbf{x}}_m^q$, but also to compute terms like $\dot{\rho}_m^q = \mathbf{e}_m^q \cdot \ddot{\mathbf{x}}_m^q$. Also, approximations of ρ_m^q and ρ_m^p are used, but the error will be small if rover position is known with an accuracy better than a few meters.

2.3 Numerical differentiation

Numerical differentiation of GNSS observables to find velocity and acceleration is an issue thoroughly studied in Bruton (2000) and Bruton et al. (1999). Several types of differentiation filters are studied there, including Taylor series expansions, Fourier series-based filters, Remez Exchange Algorithm-based filters, etc., comparing them with the ideal differentiator and weighting in their practical advantages in a GNSS data processing setting.

Relying on Bruton (2000), the filters that are used in Kennedy (2002a,b) are Finite Impulse Response (FIR)

filters because they have *linear phase*, meaning that they introduce a constant time delay that facilitates correct time-tagging of the data. In addition, only odd-length filters were used to maintain integer time delay and avoid interpolation.

Specifically, the work in Kennedy (2002b) proposes the use of a 5th order Taylor series expansion FIR filter (in this context, the filter order represents the number of samples used on either side of the central differentiator). When using a 1 Hz sampling rate, the bandwidth of that filter appropriately covers the typical dynamics found in airborne gravimetry applications, finding a compromise between bandwidth, simplicity and noise suppression (Bruton et al. 1999; Kennedy 2002b).

The impulse response of the 5th order Taylor series approximation FIR filter is shown in Eq. 21, where T is the sampling period in seconds and n represents the sample.

$$\mathbf{h}_5[n] = \frac{1}{T}\left[\frac{1}{1260} \quad \frac{-5}{504} \quad \frac{5}{84} \quad \frac{-5}{21} \quad \frac{5}{6} \quad 0 \right.$$
$$\left. \frac{-5}{6} \quad \frac{5}{21} \quad \frac{-5}{84} \quad \frac{5}{504} \quad \frac{-1}{1260}\right]. \quad (21)$$

The filter at Eq. 21 is the one to be used to find terms like $\Delta\nabla\dot{\phi}_{m,k}^{q,p}$ and $\Delta\nabla\ddot{\phi}_{m,k}^{q,p}$, as well as $\nabla\dot{\rho}_k^{q,p}$, etc.

The convolution summation is used to apply the former differentiating filter to a discrete data set $\mathbf{x}[n]$, obtaining a differenced signal $\mathbf{x}'[n]$:

$$\mathbf{x}'[i] = \sum_{j=-M}^{M} \mathbf{h}_M[j]\mathbf{x}[i-j], \quad (22)$$

where M is the order of the differentiating filter $\mathbf{h}_M[n]$. Equation 22 already compensates for the constant time delay introduced by a $2M+1$ kernel length filter.

2.4 Covariance model

Equation systems built from Eq. 13 or 20 can be solved using either Least Mean Squares or Weighted-Least Mean Squares solvers. If the latter is used, a covariance model is needed.

It can be shown (Kennedy 2002a) that a covariance model developed for carrier phase observations may be adapted to be used for carrier phase observations derivatives. Given that the numerical differentiation is a linear combination of carrier phases, then the variances can be propagated into the derivatives, as done in single and double differencing, as long as the variances are constant over the time period where the differencing filter works. When using a 1 Hz sampling rate and a 5th order FIR filter this interval is 10 s, and variances can be considered constant over that short period.

Under the former conditions, if the covariance matrix of the carrier phase observables is C_ϕ and the filter *kernel* is $\mathbf{h}[n]$, the resulting covariance matrix of the carrier phase derivatives ($C_{\dot{\phi}}$) is:

$$C_{\dot{\phi}} = \sum_0^n \mathbf{h}[n]^2 C_\phi. \quad (23)$$

And for the second carrier phase derivatives:

$$C_{\ddot{\phi}} = \left(\sum_0^n \mathbf{h}[n]^2\right)^2 C_\phi \quad (24)$$

For the covariance model itself, Kennedy (2002b) uses a model found in Radovanovic et al. (2001) which models tropospheric variances, and expands it to include ionospheric variances (Kennedy 2002a). The covariance model is elevation-based and models the physical correlations between measurements as a function of the separation angle between satellites and the baseline length between receivers.

3 Improving velocity results

Satellites' velocities and accelerations are prerequisites to apply Eqs. 13 and 20. These parameters are found in Kennedy (2002b) using analytically differentiated Lagrange polynomial functions. However, the analytical differentiation of Lagrange polynomial interpolation does not necessarily reflect the physical nature of satellite orbits. The Lagrange polynomial fit of a given set of points may yield oscillations, an effect called "*Runge phenomenon*" (see for instance Dahlquist and Bjork 1974). Those oscillations may not pose a problem when computing satellite positions from IGS products, but they may (and indeed do) introduce unwanted biases in the satellite velocity determination.

Therefore, a first modification introduced by *EVA* method consists of taking advantage of differentiator FIR filter routines used to process carrier phases to *also* compute satellite velocity and acceleration. In order to test the effects of this simple change, 5 h of data from two static (null velocity) GPS stations called UPC1 and UPC2 were processed using the full Kennedy method. Those stations are separated by a very short baseline (37.86 m), and therefore most observational errors are canceled with double differences. Data rate was 1 Hz and data was collected on 8th August 2009. The results in Fig. 2 show 5 min averages of 3D velocity errors for both approaches: Lagrange differentiator versus FIR differentiator. The 5-min averages were computed for the sake of better illustration, but no smoothing was carried out during data process.

It can be seen that the difference between using one method or the other is remarkable: The RMS of the 5-min average velocity 3D error using the Lagrange analytical differentiation is 2.52 mm/s, while the corresponding RMS value for the FIR differentiator is under 0.07 mm/s. Most of this difference comes from biases, specially in the Up
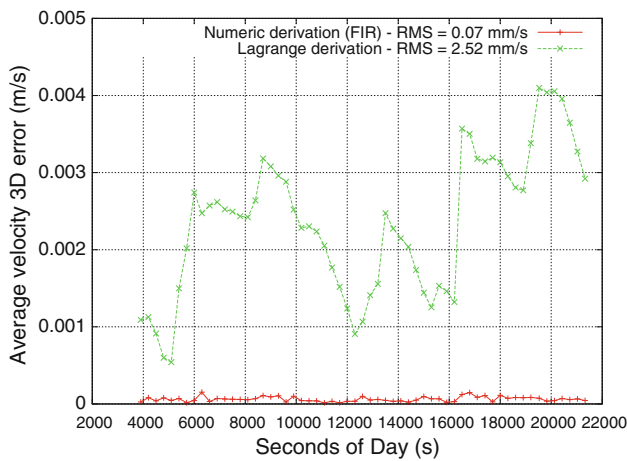
Fig. 2 Average velocity 3D error (5 min interval) for UPC2

Table 2 Velocity averages and sigmas for static results (UPC2-UPC1)

	FIR avg (mm/s)	FIR σ (mm/s)	Lagrange avg (mm/s)	Lagrange σ (mm/s)
U	0.02	3.51	−2.15	3.63
E	0.01	1.65	−0.58	1.69
N	0.00	1.68	0.51	1.76

Table 3 Acceleration averages and sigmas for static results (UPC2-UPC1)

	FIR avg (mm/s^2)	FIR σ (mm/s^2)	Lagrange avg (mm/s^2)	Lagrange σ (mm/s^2)
U	-4.0×10^{-3}	5.45	-4.2×10^{-3}	5.45
E	3.2×10^{-3}	2.57	3.2×10^{-3}	2.57
N	0.7×10^{-3}	2.61	0.3×10^{-3}	2.61

velocity component. Table 2 presents the averages and standard deviations for Up, East and North components for both approaches.

The results for acceleration yield negligible differences when using one method or the other, as Table 3 shows. This may be explained by looking back at Eq. 20, where relative velocity errors are scaled down by a factor of ρ_m^{SV}, which is a very large value. This is further explained in Kennedy (2002a).

Regarding results in Tables 2 and 3 (and all subsequent velocity and acceleration results shown in this work), it is important to emphasize that these are *unfiltered*, 1 Hz results. For airborne gravimetry purposes it is an usual practice to filter the acceleration results, depending on the desired spatial resolution of the gravity field. For a typical aircraft speed of 45 m/s, filter periods range from 30 to 120 s, yielding spatial resolutions from 0.7 to 2.7 km (Kennedy 2002a).

Table 4 Velocity and accelerations results for PLAN-EBRE using numerical derivation (FIR filter) (static test)

	Average	Velocity σ	
V_U	−0.13	4.47	(mm/s)
V_E	0.06	2.22	(mm/s)
V_N	0.03	2.42	(mm/s)
A_U	3.3×10^{-3}	6.92	(mm/s^2)
A_E	2.4×10^{-3}	3.43	(mm/s^2)
A_N	-4.2×10^{-3}	3.76	(mm/s^2)

Please note that the static error sigmas for velocities in the FIR case (Table 2) are below what is reported by van Graas and Soloviev (2004) (Table 1). Therefore, a longer baseline should be examined to see if good results are obtained over larger separation distances.

In order to test the former hypothesis, 3 h of data at 1 Hz data rate were processed for receivers PLAN (*rover*) and EBRE (*reference*) for 15th January 2010. The baseline between those receivers is 142 km. Table 4 presents the results for this longer baseline. It can be seen that although the results are not as good as the ones with the very short baseline (as expected), they still show consistently better sigmas than van Graas and Soloviev (2004) static velocity results, specially in the Up direction (Table 1).

3.1 Modifications to covariance model

It was decided that for the new *EVA* method, as well as the modified Kennedy method, the original Kennedy covariance model would be partially used: only terms corresponding to the main diagonal will be taken into account. The use of simple diagonal covariance models is a common practice in navigation (see, for instance, Walter et al. 1997). These models are very useful, fast, and easily adapt to a variety of conditions.

In this case, the choice of a diagonal covariance model is further reinforced by the fact that that *EVA* method focuses on long baselines, and therefore the tropospheric conditions at distant receivers are completely decorrelated, while the ionospheric conditions are either decorrelated or weakly decorrelated, depending on ionosphere state. Under this situation, the cross-correlation terms in the covariance model tend to zero, leaving a diagonal matrix. Moreover, it must also be taken into account that for very long baselines the *EVA* method suggest using the ionosphere-free carrier phase observables (LC), further reinforcing complete measurement decorrelation.

An additional issue to consider is that the original Kennedy covariance model indeed does not model the covariance terms in an appropriate way, because it assigns the same

correlation distance to troposphere and ionosphere, being well known that they have very different correlation distances. In summary, the original covariance method introduces cross-correlation terms that should not be included, and does it in an incorrect way. Indeed, Kennedy (2002a) states:

Further refinements in the covariance model are definitely possible. However, the focus on this thesis is the comparison of the carrier and position methods of acceleration determination. An adequate, but not necessarily ideal, covariance model is required for testing the carrier method. The covariance model developed herein provided reasonable results and was deemed adequate for the purposes at hand.

Given the aforementioned issues, it is considered that a simpler diagonal covariance model is more appropriate for the conditions *EVA* method was developed for. It is out of the scope of this work to evaluate the best covariance model to use with the carrier phase-based method of velocity and acceleration determination. However, assessing simpler alternatives for these covariance models is suggested as a future research line.

4 Extended velocity and acceleration determination

Kennedy's method uses L1 carrier phase observable due to its lower noise, and relies on double differencing to eliminate or minimize error sources like satellite clock drifts. The following sections will present modifications to this method where clock drift and clock drift rates are estimated on the fly, and will henceforth be called "*Extended velocity and acceleration determination* (*EVA*)".

4.1 Computing the velocity

Considering a reference satellite q, Eq. 5 may be rewritten as:

$$\dot{\rho}_m^q - \mathbf{e}_m^q \cdot \dot{\mathbf{x}}^q = -\mathbf{e}_m^q \cdot \dot{\mathbf{x}}_m. \tag{25}$$

The objective is to find a way to estimate the term $\dot{\rho}_m^q$. In order to achieve that, a *reference clock* dt_0 is introduced to which all the other clocks will refer to. Hence:

$$d\tau_m = dt_m - dt_0$$
$$d\tau^q = dt^q - dt_0.$$

And Eq. 9 becomes:

$$\phi_m^q - rel_m^q - T_m^q - \omega_{\phi,m}^q$$
$$= \rho_m^q + c(d\tau_m - d\tau^q) + \delta T_m^q - \alpha_f I_m^p + b_m^q$$
$$+ m_{\phi,m}^q + \varepsilon_{\phi,m}^q, \tag{26}$$

where terms to the left are the observation minus modelable effects, and they will be denoted as $\phi_{0,m}^q$. Arranging terms it yields:

$$\rho_m^q = \phi_{0,m}^q - c(d\tau_m - d\tau^q) - \delta T_m^q + \alpha_f I_m^p - b_m^q - \varepsilon_{\phi,m}^q, \tag{27}$$

where term $m_{\phi,m}^q$ is considered as absorbed into $\varepsilon_{\phi,m}^q$. Differentiating Eq. 27 regarding time, and assuming that no cycle slip occurs, results in Eq. 28.

$$\dot{\rho}_m^q = \dot{\phi}_{0,m}^q - cd\dot{\tau}_m + cd\dot{\tau}^q - \delta \dot{T}_m^q + \alpha_f \dot{I}_m^p - \dot{\varepsilon}_{\phi,m}^q. \tag{28}$$

Equation 28 could be considered as equivalent to equation 6.33 found in Misra and Enge (2006). If it is further considered that troposphere and ionosphere variation rates are negligible with respect to rover velocity, as well as other first order errors, then:

$$\dot{\rho}_m^q \simeq \dot{\phi}_{0,m}^q - cd\dot{\tau}_m + cd\dot{\tau}^q. \tag{29}$$

For Eq. 29 to be valid, receiver clock millisecond adjustments must be taken care of, either by preprocessing RINEX observation files or by using clock steering-style receivers. With this assumption, combining Eq. 29 with Eq. 25 results into the new equation for rover velocity estimation:

$$\dot{\phi}_{0,m}^q - \mathbf{e}_m^q \cdot \dot{\mathbf{x}}^q = -\mathbf{e}_m^q \cdot \dot{\mathbf{x}}_m + cd\dot{\tau}_m - cd\dot{\tau}^q. \tag{30}$$

The unknowns in the former equation are the rover velocity $\dot{\mathbf{x}}_m$, the rover clock drift $cd\dot{\tau}_m$, and the satellite clock drift $cd\dot{\tau}^q$.

Let us now introduce a fixed *master* station "0". The receiver clock of this station is the reference clock dt_0 introduced earlier. Then, Eq. 30 for *master* station becomes:

$$\dot{\phi}_{0,0}^q - \mathbf{e}_0^q \cdot \dot{\mathbf{x}}^q = -cd\dot{\tau}^q. \tag{31}$$

As it can be seen, the equations corresponding to *master* station allow to estimate satellite clock drifts (in fact, satellite clock drifts with respect to *master* station clock drift). Following the same procedure, let's introduce some *reference* stations denoted with "k", where the equations provided by these reference stations reinforce the estimation of satellite clock drifts:

$$\dot{\phi}_{k,m}^q - \mathbf{e}_k^q \cdot \dot{\mathbf{x}}^q = cd\dot{\tau}_k - cd\dot{\tau}^q. \tag{32}$$

Finally, Eqs. 30–32 allow to build an equation system suitable to be solved using the GPSTk `SolverGeneral` class, as explained for the *Precise Orbits Positioning* (POP) strategy in Salazar et al. (2010).

4.2 Computing the acceleration

From Eq. 17, we have for a satellite q that:

$$\ddot{\rho}_m^q - \mathbf{e}_m^q \cdot \ddot{\mathbf{x}}^q - \frac{1}{\rho_m^q}\left[|\dot{\mathbf{x}}_m^q|^2 - (\dot{\rho}_m^q)^2\right] = -\mathbf{e}_m^q \cdot \ddot{\mathbf{x}}_m. \tag{33}$$

On the other hand, further differentiating Eq. 29 regarding time yields:

$$\ddot{\rho}_m^q \simeq \ddot{\phi}_{0,m}^q - cd\dddot{\tau}_m + cd\dddot{\tau}^q. \tag{34}$$

Combining Eqs. 33 and 34, the new equation to estimate rover acceleration is obtained:

$$\ddot{\phi}_{0,m}^q - \mathbf{e}_m^q \cdot \ddot{\mathbf{x}}^q - \frac{1}{\rho_m^q} \left[|\dot{\mathbf{x}}_m^q|^2 - \left(\dot{\rho}_m^q\right)^2 \right]$$
$$= -\mathbf{e}_m^q \cdot \ddot{\mathbf{x}}_m + cd\ddot{\tau}_m - cd\ddot{\tau}^q. \tag{35}$$

Introducing again a *master* station "0" and several *reference* stations "*k*":

$$\ddot{\phi}_{0,0}^q - \mathbf{e}_0^q \cdot \ddot{\mathbf{x}}^q - \frac{1}{\rho_0^q} \left[|\dot{\mathbf{x}}^q|^2 - (\dot{\rho}_0^q)^2 \right] = -cd\ddot{\tau}^q \tag{36}$$

$$\ddot{\phi}_{0,k}^q - \mathbf{e}_k^q \cdot \ddot{\mathbf{x}}^q - \frac{1}{\rho_k^q} \left[|\dot{\mathbf{x}}^q|^2 - (\dot{\rho}_k^q)^2 \right] = cd\ddot{\tau}_k - cd\ddot{\tau}^q. \tag{37}$$

The former equation system can also be solved using the GPSTk `SolverGeneral` class.

5 Applying *EVA* method to aircraft data

An application of the *EVA* method to aircraft velocity and acceleration determination was tested. The data comes from the flight of a light aircraft from Perpignan airport, south of France, to La Cerdenya aerodrome, in the Spanish Pyrenees, with a previous pass close to Llivia aerodrome. The distance from Perpignan to Llivia is about 79 km, and the distance between Llivia and La Cerdenya is 13 km.

This experiment used GPS data from five (5) Institut Cartografic de Catalunya (ICC) reference stations: AVEL, CREU, EBRE, LLIV and MATA (see Fig. 3), all of them using two-frequency geodetic-grade Trimble NETRS receivers with geodetic-grade antennas (models TRM29659.00 and TRM41249.00). The LLIV (Llivia) station is *not* used for *EVA* method data processing, it is saved for independent reference determination purposes with Kennedy's method. The remaining four-station network has MATA as the closest station to LLIV, 111 km away. It is important to note that the Kennedy method used for comparisons is the modified version according to Sect. 3.

5.1 Aircraft description

The aircraft used was a *Robin DR 400-140B*, shown in Fig. 4. This is a light airplane with some properties that make it very appropriate for this kind of experiments: It is a low-wing aircraft, with an excellent sky view from the cockpit, most of the cockpit roof is made of Plexiglas, transparent to radiowaves, and most of the aircraft structure is made of wood and fabric instead of metal, minimizing multipath.
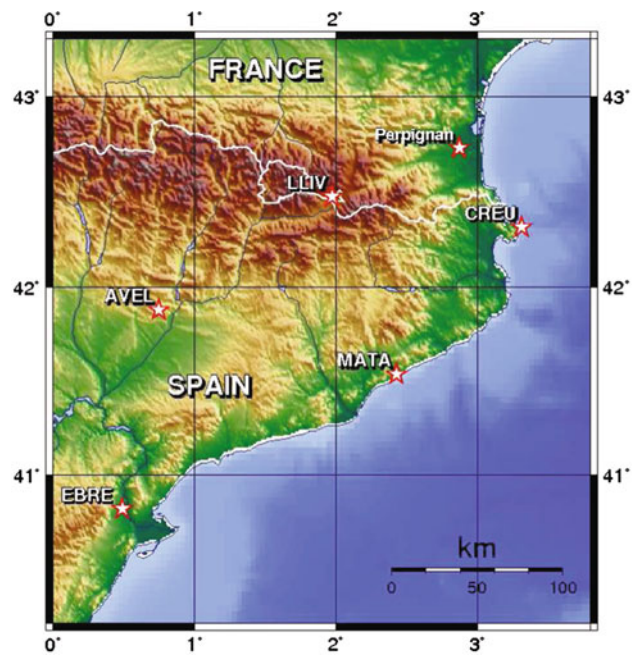

Fig. 3 Station network for Pyrenees flight

Fig. 4 Aircraft Robin DR400-140B

Regarding the data collection process, the rover receiver was a two-frequency geodetic-grade *Septentrio PolaRx2*, the antenna was a two-frequency one (model AERAT2775_43), and it was attached on the upper right side of the instrument panel, inside the cockpit. The test flight was carried out on 21st March 2009, under Visual Flight Rules (VFR) with clear skies along the flight path, lasting a little over 1 hour (from 11:36 to 12:40, local time).

5.2 Aircraft data processing

In order to process data with the *EVA* method the aircraft *a priori* position has to be updated each epoch. For this, the ionosphere-free pseudorange observable smoothed with the ionosphere-free carrier phase, was used at each epoch to generate an approximate position, which would then be used as
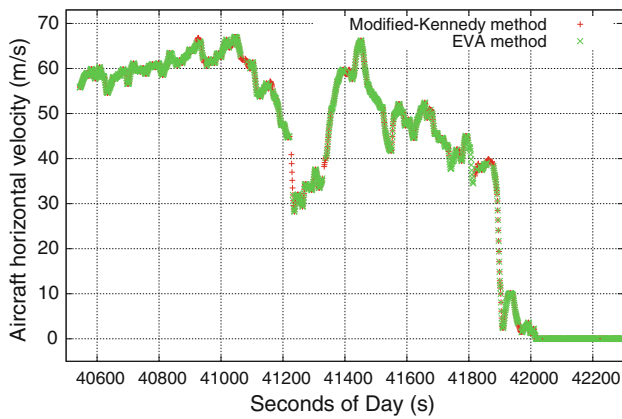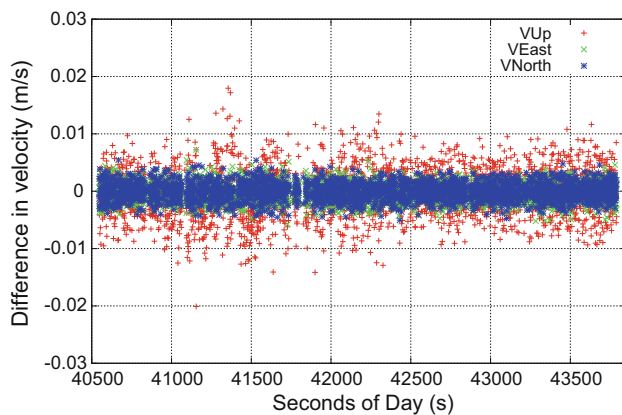
Fig. 5 Aircraft horizontal velocity

Fig. 6 Aircraft velocity differences of *EVA* with respect to modified-Kennedy. Kinematic and static flight phases

Fig. 7 Aircraft vertical velocity during static flight phase

Table 5 Aircraft velocity and acceleration averages and sigmas for static period, "Up" component

Component	Modified-Kennedy	EVA	RTK
V_U avg (mm/s)	−0.015	0.186	0.002
V_U σ (mm/s)	4.447	3.720	4.887
A_U avg (mm/s^2)	−0.017	0.001	0.020
A_U σ (mm/s^2)	6.750	5.670	7.945

a priori for the modeling phase. The rest of the procedure follows the explanation in Sect. 4.

On the other hand, the Kennedy method was also implemented but included the improvements proposed in Sect. 3 (i.e., FIR filter instead of Lagrange differentiator to compute satellite orbits, and a simpler covariance model), and called hereafter modified-Kennedy. The fixed LLIV station was used as reference. It is important to remark here that the data was processed when the aircraft was relatively close to LLIV (less than 37 km). Figure 5 shows the results for aircraft horizontal velocity using both approaches. There is very good agreement, and the apparent differences in the plot are due to areas where one method is providing solutions while the other is not. The flat area at lower right is because the aircraft had already landed and was parked.

Figure 6 plots the differences in velocities of *EVA* with respect to modified-Kennedy for the three coordinates, both for the kinematic and static parts of the flight. The standard deviation of velocity differences is 4.1 mm/s for the "Up" component, 1.6 mm/s for the "East", and 1.5 mm/s for the "North" velocity difference component. Regarding
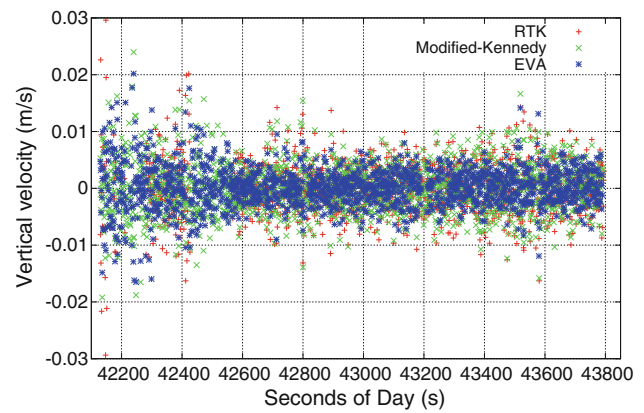
acceleration, the corresponding standard deviation values are 6.2 mm/s^2 (Up) and both 2.4 mm/s^2 for both East and North. This is a very good agreement, especially taking into account the long baseline length of the *EVA* approach.

The "reference truth" for a kinematic tests of this type is very difficult to establish. Several methods has been tried to provide reference values (see, for instance, Kennedy 2002a and Zhang and Forsberg 2007), but further research in this field is necessary. Therefore, a better way to assess the results of each method is to study the period of time when the aircraft is parked at La Cerdenya airport, 13 km from the LLIV reference station. This period spans from second of day 42,130–43,790 s. For comparison purposes, a Real-Time Kinematic (RTK) solution was generated with the RTKLIB tool (Takasu and Yasuda 2009) was also included. The RTK solution was twice numerically differenced using the FIR filter described in Sect. 2.3 in order to obtain both velocity and acceleration reference values. The LLIV station was also used as fixed station for the RTK procedure.

As Fig. 7 shows, the vertical velocities yielded by the three methods are comparable when using a known zero reference velocity. The *EVA* method produces the best velocity estimates. The acceleration estimates are similar, although the *EVA* method again shows a significant advantage. Table 5 presents a summary of average and standard deviations for the "Up" components during the static period.

Overall, it can be said that the use of a network of stations (*EVA* method) tends to reduce the standard deviation,

Table 6 South America network data

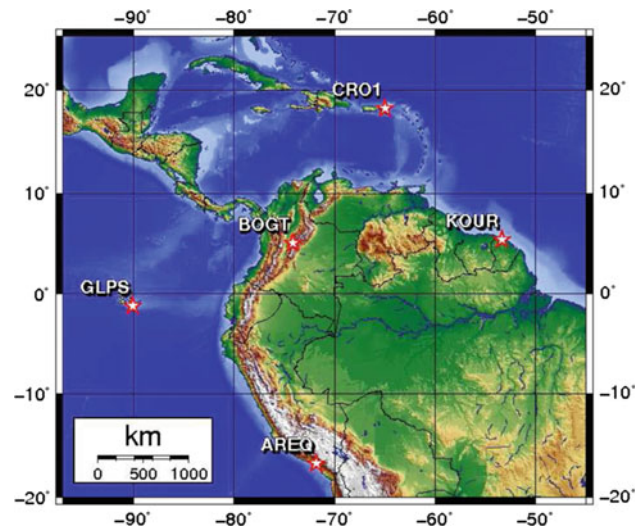| Station	Latitude	Longitude	Distance to BOGT (km)
AREQ	−16.47°	−71.49°	2,339
BOGT	4.64°	−74.08°	–
CRO1	17.76°	−64.58°	1,777
GLPS	−0.74°	−90.3°	1,893
KOUR	5.25°	−52.81°	2,347

Fig. 8 South America network

while the distance between rover and nearest reference station increased the biases in velocity. Also, both the modified-Kennedy and *EVA* outperform RTK in acceleration estimation. All studied methods have better performance than van Graas and Soloviev (2004) (Table 1).

6 Applying *EVA* method to very long ranges

The previous section compared *EVA* method performance with differential methods when there was a reference station near the working area. However, the purpose of *EVA* method is to provide velocity and acceleration estimations when there is no nearby reference station. It is in this scenario where *EVA* method has important advantages.

In order to test the *EVA* method in a demanding setting, a very wide area in equatorial South America was processed, using 1 Hz data acquired on 15th January 2010, from 19:00 to 20:00 UT (about local noon). The processed network had 5 stations, using BOGT as "*rover*" and station CRO1 as "*master*". Table 6 shows station data, while Fig. 8 presents a map of this network.

The modified-Kennedy method was used for comparison purposes taking station CRO1 as reference. Table 7 shows

Table 7 Velocity and accelerations results for BOGT-CRO1: Modified-Kennedy method (static test)

Component	Average	Sigma	
V_U	0.54	6.90	(mm/s)
V_E	0.67	2.31	(mm/s)
V_N	0.48	4.74	(mm/s)
A_U	0.6×10^{-3}	10.27	(mm/s²)
A_E	1.8×10^{-3}	3.34	(mm/s²)
A_N	6.8×10^{-3}	7.08	(mm/s²)

Table 8 Velocity and accelerations results as function of network size (including *rover*) for BOGT: *EVA* method (static test)

Network	Component	Average	Sigma	
	V_U	0.10	6.74	(mm/s)
(2)	V_E	0.14	2.16	(mm/s)
BOGT	V_N	0.30	4.65	(mm/s)
CRO1	A_U	8.6×10^{-3}	10.23	(mm/s²)
	A_E	9.7×10^{-3}	3.27	(mm/s²)
	A_N	4.1×10^{-3}	7.02	(mm/s²)
	V_U	−0.73	1.51	(mm/s)
(3)	V_E	−0.51	1.18	(mm/s)
AREQ	V_N	0.33	0.92	(mm/s)
BOGT	A_U	-1.0×10^{-3}	2.26	(mm/s²)
CRO1	A_E	5.9×10^{-3}	1.74	(mm/s²)
	A_N	-1.7×10^{-3}	1.38	(mm/s²)
	V_U	−0.59	1.48	(mm/s)
(4)	V_E	−0.66	1.16	(mm/s)
AREQ	V_N	0.36	0.88	(mm/s)
BOGT	A_U	-2.3×10^{-3}	2.21	(mm/s²)
CRO1	A_E	4.0×10^{-3}	1.72	(mm/s²)
GLPS	A_N	-2.7×10^{-3}	1.32	(mm/s²)
(5)	V_U	−0.63	1.43	(mm/s)
AREQ	V_E	−0.58	1.13	(mm/s)
BOGT	V_N	0.35	0.83	(mm/s)
CRO1	A_U	-4.9×10^{-3}	2.13	(mm/s²)
GLPS	A_E	5.4×10^{-3}	1.65	(mm/s²)
KOUR	A_N	-2.0×10^{-3}	1.24	(mm/s²)

the results for velocity and acceleration when using modified-Kennedy method, while Table 8 presents *EVA* method results when using networks of 2–5 stations.

It can be seen that given the distances, the latitude, and the time of day involved, modified-Kennedy method results are nearly identical to the 2 station *EVA* results, but the results obtained with the *EVA* method are considerably better when additional base stations are introduced. This is reinforced when the vertical velocity component is plotted for both methods, as Fig. 9 shows. The *EVA* method has con-
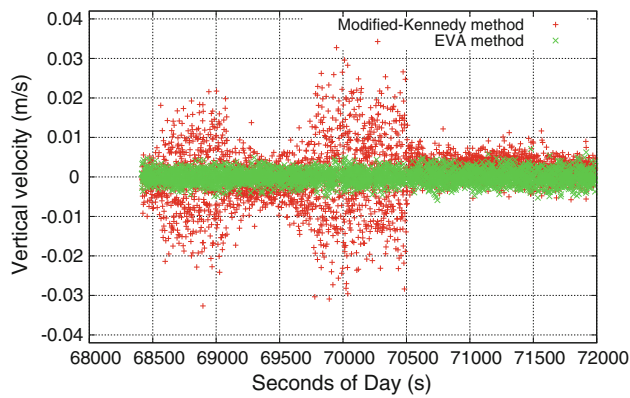
Fig. 9 Vertical velocity for BOGT station. *EVA* method uses a 5-station network. Static test

siderable less dispersion and also shows less bias. The same behavior is observed for the rest of the velocity and acceleration components. This improvement is mainly due to the improved geometry provided by the network, as commented in Sect. 6.1.

6.1 Effect of the improved geometry

In order to show the effects of the improved geometry provided by using a network of reference stations we can compare the results obtained using networks involving from 2 up to 5 stations (including the *rover*), as presented in Table 8. It can be seen that the increase in network size yields a significant improvement in the results, specially regarding the dispersion value, with the biggest improvements appearing when changing from a 2-station network to 3 stations. Indeed, results obtained when using 3 or more stations are comparable.

The improved geometry of a wider network allows a better estimation of the unknown values, in particular the satellite clock offsets, providing more robust results. On the other hand, a 2-station network strategy (whether modified-Kennedy or *EVA*) may not have enough common satellites to properly estimate the unknowns, rendering the network results vulnerable to the appearance or disappearance of satellites. This can be observed at second of day 70,498 in Fig. 9 for the modified-Kennedy method, where satellite PRN27 enters the solution and yields a notable improvement, whereas a 5-station *EVA* approach provides more consistent results across the entire time range.

6.2 Effect of the ionosphere-free observable

Table 9 shows the results of repeating the previous computations for the South American network, but using LC (ionosphere-free phase combination) instead of L1 as main observable.

Table 9 Velocity and accelerations results as function of network size (including *rover*) for BOGT: *EVA* method with LC (static test)

Network	Component	Average	Sigma	
	V_U	0.02	8.35	(mm/s)
(2)	V_E	−0.05	2.71	(mm/s)
BOGT	V_N	0.07	5.95	(mm/s)
CRO1	A_U	0.02	11.39	(mm/s^2)
	A_E	0.01	3.77	(mm/s^2)
	A_N	0.01	8.00	(mm/s^2)
	V_U	−0.03	1.79	(mm/s)
(3)	V_E	0.02	1.39	(mm/s)
AREQ	V_N	−0.04	1.08	(mm/s)
BOGT	A_U	-3.7×10^{-3}	2.52	(mm/s^2)
CRO1	A_E	7.2×10^{-3}	1.95	(mm/s^2)
	A_N	-1.8×10^{-3}	1.54	(mm/s^2)
	V_U	−0.03	1.73	(mm/s)
(4)	V_E	0.02	1.34	(mm/s)
AREQ	V_N	−0.03	1.01	(mm/s)
BOGT	A_U	-4.0×10^{-3}	2.45	(mm/s^2)
CRO1	A_E	4.7×10^{-3}	1.90	(mm/s^2)
GLPS	A_N	-3.6×10^{-3}	1.44	(mm/s^2)
(5)	V_U	-9.5×10^{-3}	1.67	(mm/s)
AREQ	V_E	0.02	1.29	(mm/s)
BOGT	V_N	−0.02	0.95	(mm/s)
CRO1	A_U	-6.3×10^{-3}	2.37	(mm/s^2)
GLPS	A_E	5.6×10^{-3}	1.84	(mm/s^2)
KOUR	A_N	-2.7×10^{-3}	1.35	(mm/s^2)

It can be seen that using an observable with higher noise such as LC leads to a small increase in dispersion (around 15%), but on the other hand there is an order of magnitude improvement in biases for the velocity results. This indicates that ionospheric drift may affect velocity determination under the conditions of this experiment. On the other hand, L1-based bias and dispersion results for acceleration are always better, suggesting that ionospheric drift rate plays a minor role in acceleration computation.

Table 10 presents the 3DRMS values for velocity and acceleration determination using both L1 and LC. This table shows that, overall, it may be better to use the L1 observable for both velocity and acceleration determination, unless lower biases in velocity determination are of importance, or when high ionospheric gradients are expected.

6.3 Effect of the quality of orbital data

For the results presented so far, only final precise orbits products provided by the International GNSS Service (IGS) have been used. In the past 15 years the accuracy of IGS final orbital products have improved enormously, from about 30 cm

Table 10 BOGT station 3DRMS for EVA method estimation of velocity (mm/s) and acceleration (mm/s^2) as function of network size and different strategies (static test)

Size	Parameter	3DRMS L1	3DRMS LC	3DRMS Predicted
2	V	8.48	10.61	15.90
	A	12.83	14.42	24.08
3	V	2.32	2.51	2.80
	A	3.17	3.54	3.47
4	V	2.29	2.41	2.77
	A	3.10	3.42	3.36
5	V	2.21	2.32	2.66
	A	2.97	3.28	3.20

Table 11 Velocity and accelerations results as function of network size (including *rover*) for BOGT: *EVA* method with L1 and Ultra-rapid (predicted) orbital products (static test)

Network	Component	Average	Sigma	
	V_U	-0.29	13.06	(mm/s)
(2)	V_E	-0.13	4.28	(mm/s)
BOGT	V_N	0.26	8.00	(mm/s)
CRO1	A_U	0.03	19.76	(mm/s^2)
	A_E	0.02	6.47	(mm/s^2)
	A_N	0.02	12.15	(mm/s^2)
	V_U	-0.97	1.64	(mm/s)
(3)	V_E	-0.95	1.29	(mm/s)
AREQ	V_N	0.75	1.04	(mm/s)
BOGT	A_U	-2.9×10^{-3}	2.45	(mm/s^2)
CRO1	A_E	4.9×10^{-3}	1.90	(mm/s^2)
	A_N	-0.6×10^{-3}	1.55	(mm/s^2)
	V_U	-0.83	1.59	(mm/s)
(4)	V_E	-1.08	1.26	(mm/s)
AREQ	V_N	0.83	1.02	(mm/s)
BOGT	A_U	-4.9×10^{-3}	2.36	(mm/s^2)
CRO1	A_E	2.5×10^{-3}	1.85	(mm/s^2)
GLPS	A_N	-1.1×10^{-3}	1.52	(mm/s^2)
(5)	V_U	-0.88	1.52	(mm/s)
AREQ	V_E	-1.00	1.22	(mm/s)
BOGT	V_N	0.80	0.95	(mm/s)
CRO1	A_U	-6.2×10^{-3}	2.26	(mm/s^2)
GLPS	A_E	3.8×10^{-3}	1.79	(mm/s^2)
KOUR	A_N	-1.3×10^{-3}	1.41	(mm/s^2)

to 1–2 cm (Kouba 2009). However, big improvements have also been achieved in the other IGS products, namely: Rapid, Ultra-Rapid (observed) and Ultra-Rapid (predicted).

With respect to the Ultra-Rapid (predicted) products, the current challenge mainly lies in the satellite clock predictions. The IGS reports that the orbital information achieves an accuracy of about 5 cm. Considering that the EVA method only uses orbital data and disregards clock data, an interesting question was how the EVA method performs when predicted products were used.

Table 11 shows the results obtained when using L1 observations and Ultra-rapid (predicted) IGS products instead of Final ones for the same Bogota network. When comparing these results with Table 8, a decrease on accuracy is shown (as expected). However, this decrease is relatively small (at most 16% increase in standard deviation) for the cases when 4 or more stations are used. In some cases, the L1-based Ultra-Rapid results are better than those using Final IGS products and the LC observable (Table 9). Table 10 summarizes these comparisons using the 3DRMS figures.

Overall, Table 10 shows that the 3DRMS acceleration results obtained using L1 and Ultra-Rapid (predicted) products are better than the ones obtained with LC combination and Final products for network sizes 3 or bigger, while the 3DRMS velocity results are under 15% worse for the same network sizes. The former suggests that Ultra-Rapid (predicted) products are a valid alternative to obtain reasonably good velocity and acceleration estimates in a very short time.

7 Conclusions

In this work a new carrier phase-based velocity and acceleration determination method is presented that uses L1 carrier phase observables for velocity and acceleration determination and a network of stations to estimate satellite clock drifts and drift rates 'on-the-fly'. This approach is independent of precise clock information and greatly extends the effective

baseline of previous similar techniques. This method was named 'Extended velocity and acceleration determination' (EVA).

The EVA method could be considered as an extension of the carrier phase-based Kennedy method, whose fundamentals were reviewed. During the development of this work, some problems were found in the velocity estimation process of the Kennedy method, the sources of these problems were identified, and an improved version of the Kennedy method was used during the remaining of this research work. It should be noted, however, that the original Kennedy method was initially only concerned with precise acceleration determination.

While the Kennedy method relies on double differencing to eliminate or minimize error sources such as satellite clock drifts and drift rates, EVA uses a network of stations to estimate those parameters 'on-the-fly', and thence it only needs orbit data of certain quality to work. The overall results obtained with EVA show that for long baselines the network-based estimation dramatically reduces the dispersion

and improves the robustness. The main reason for this is the better geometry provided by the network of stations.

The EVA technique may also use the undifferenced ionosphere-free carrier phase combination (LC), overcoming baseline limitations in those cases when ionosphere gradients may be an issue and very low biases are required for velocity results, at the expense of higher sigmas and RMS.

Another issue addressed in this work was the overall effect of the quality of orbital data used in the EVA method. The EVA method doesn't require precise clock information, and therefore it is not limited to using only the Final IGS products. The results showed a small (under 15%) degradation for network sizes of 3 or bigger when Ultra-Rapid (predicted) products were used, which may be acceptable when minimum latency is the priority and near real-time results are required.

An experiment was setup using a light aircraft flying over the Pyrenees, showing that both EVA and improved Kennedy methods are able to cope with mountainous flight dynamics. An additional RTK-derived solution was also generated, and when comparing the three methods to a known zero-velocity reference the results were very similar and yielded excellent performance. The EVA method and the improved-Kennedy method outperformed the RTK-derived solutions, and the EVA method provided the best results in this scenario in spite of the fact that the nearest reference station was more than one hundred kilometers away.

Finally, the improved-Kennedy and EVA methods were applied to a network on equatorial South America with baselines over 1,770 km. Under this scenario, the EVA method showed a clear advantage for all components of velocity and acceleration.

The software used to process experimental data was developed using the GPSTk open source library, and open implementations of EVA algorithms will be added to the GPSTk software repository (see ARL 2010).

References

ARL (2010) The GPS Toolkit, GPSTk [Online; accessed November 20th, 2010]. http://www.gpstk.org/

Bruton AM (2000) Improving the accuracy and resolution of SINS/DGPS airborne gravimetry. PhD thesis. Department of Geomatics Engineering, University of Calgary, Calgary, Alberta, Canada. Report No. 20145

Bruton AM, Glennie CL, Schwarz KP (1999) Differentiation for high-precision GPS velocity and acceleration determination. GPS Solut 2(4):7–21

Cannon ME, Lachapelle G, Szarmes MC, Hebert JM, Keith J, Jokerst S (1997) DGPS kinematic carrier phase signal simulation analysis for precise velocity and position determination. J Inst Navig 44(2):231–246

Dahlquist G, Bjork A (1974) Numerical methods. Prentice Hall, Englewood Cliffs. ISBN 0-13-627315-7

Hofmann-Wellenhof B, Lichtenegger KH, Wasle E (2008) GNSS—Global navigation satellite systems. Springer, Wien

Jekeli C (1994) On the computation of vehicle accelerations using GPS phase accelerations. In: Proceedings of the international symposium on kinematic systems in geodesy, geomatics and navigation (KIS94), Banff, Canada, pp 473–481

Jekeli C, Garcia R (1997) GPS phase accelerations for moving-base vector gravimetry. J Geodesy 71(10):630–639. doi:10.1007/s001900050130

Kennedy S (2002a) Acceleration estimation from GPS carrier phases for airborne gravimetry Master's thesis. Department of Geomatics Engineering, University of Calgary, Calgary, Alberta, Canada report no. 20160

Kennedy S (2002b) Precise acceleration determination from carrier phase measurements. In: Proceedings of the 15th international technical meeting of the satellite division of the Institute of Navigation. ION GPS 2002, Portland, pp 962–972

Kouba J (2009) A guide to using International GNSS Service (IGS) products. Tech. rep., International GNSS Service, http://acc.igs.org/UsingIGSProductsVer21.pdf

Misra P, Enge P (2006) Global positioning system. Signals, measurements and performance. Ganga-Jamuna Press, USA

Parkinson BW, Spilker Jr JJ (1996) Global positioning system: theory and applications, vol I & II. American Institute for Aeronautics and Astronautics, USA

Radovanovic RS, El-Sheimy N, Teskey W (2001) Rigorous combination of GPS data from multiple base stations for mobile platform positioning. In: Proceedings of the 3rd international symposium on mobile mapping technology, Cairo, Egypt

Salazar D, Hernandez-Pajares M, Juan J, Sanz J (2010) GNSS data management and processing with the GPSTk. GPS Solut 14(3): 293–299. doi:10.1007/s10291-009-0149-9

Szarmes M, Ryan S, Lachapelle G, Fenton P (1997) DGPS high accuracy aircraft velocity determination using Doppler measurements. In: Proceedings of the international symposium on kinematic systems (KIS97), Banff, Alberta, Canada

Takasu T, Yasuda A (2009) Development of the low-cost RTK-GPS receiver with an open source program package rtklib. In: Proceedings of international symposium on GPS/GNSS, Jeju, Korea

van Graas F, Soloviev A (2004) Precise velocity estimation using a stand-alone GPS receiver. NAVIGATION. J Inst Navig 51(4):283–292

Walter T, Enge P, Hansen A (1997) A proposed integrity equation for WAAS MOPS. In: Proceedings of the 10th international technical meeting of the Satellite Division of The Institute of Navigation (ION GPS 1997), Kansas City, USA, pp 475–484

Zhang X, Forsberg R (2007) Assessment of long-range kinematic GPS positioning errors by comparison with airborne laser altimetry and satellite altimetry. J Geodesy 81(3):210–211. doi:10.1007/s00190-006-0100-6